



HAL
open science

Titan: Atmospheric and surface features as observed with Nasmyth Adaptive Optics System Near-Infrared Imager and Spectrograph at the time of the Huygens mission

Mathieu Hirtzig, A. Coustenis, E. Gendron, P. Drossart, M. Hartung, A. Negrão, Pascal Rannou, M. Combes

► To cite this version:

Mathieu Hirtzig, A. Coustenis, E. Gendron, P. Drossart, M. Hartung, et al.. Titan: Atmospheric and surface features as observed with Nasmyth Adaptive Optics System Near-Infrared Imager and Spectrograph at the time of the Huygens mission. *Journal of Geophysical Research. Planets*, 2007, 112, pp.E02S91. 10.1029/2005JE002650 . hal-00162016

HAL Id: hal-00162016

<https://hal.science/hal-00162016>

Submitted on 3 Dec 2020

HAL is a multi-disciplinary open access archive for the deposit and dissemination of scientific research documents, whether they are published or not. The documents may come from teaching and research institutions in France or abroad, or from public or private research centers.

L'archive ouverte pluridisciplinaire **HAL**, est destinée au dépôt et à la diffusion de documents scientifiques de niveau recherche, publiés ou non, émanant des établissements d'enseignement et de recherche français ou étrangers, des laboratoires publics ou privés.

Titan: Atmospheric and surface features as observed with Nasmyth Adaptive Optics System Near-Infrared Imager and Spectrograph at the time of the Huygens mission

M. Hirtzig,^{1,2} A. Coustenis,² E. Gendron,² P. Drossart,² M. Hartung,⁴ A. Negrão,^{2,3} P. Rannou,^{2,3} and M. Combes²

Received 25 November 2005; revised 13 July 2006; accepted 14 September 2006; published 14 February 2007.

[1] At the time of the Huygens probe descent in Titan's atmosphere, on 14 January 2005, many ground-based telescopes were pointed toward Saturn's satellite. Here, we describe the data collected on 15 and 16 January with Nasmyth Adaptive Optics System Near-Infrared Imager and Spectrograph (NACO) at the Very Large Telescope. We acquired adaptive optics images in the near-infrared in several NACO modes, 18 then 41 hours after Huygens landing. A variety of different filters, a cryogenic tunable Fabry-Perot interferometer, and a simultaneous differential imager were used. All these data allowed us to construct a diagnostic of the appearance of Titan's atmosphere and surface at the time of the Huygens probe's descent. We describe the north-south and east-west asymmetries characterizing the atmosphere, while reporting on more active phenomena, like cloud activity. The surface of Titan around the Huygens probe's landing site is imaged with a 320-km spatial resolution, through three methane windows at 1.28, 1.6, and 2.0 μm ; it shows features similar to those previously published in near-infrared maps, with a spectral behavior compatible with methane and water ices.

Citation: Hirtzig, M., A. Coustenis, E. Gendron, P. Drossart, M. Hartung, A. Negrão, P. Rannou, and M. Combes (2007), Titan: Atmospheric and surface features as observed with Nasmyth Adaptive Optics System Near-Infrared Imager and Spectrograph at the time of the Huygens mission, *J. Geophys. Res.*, *112*, E02S91, doi:10.1029/2005JE002650.

1. Introduction

[2] Ever since the first images taken in 1992 [*Saint-Pé et al.*, 1993], adaptive optics proved to be an efficient way to compensate for the Earth's atmospheric turbulence, allowing astronomers to resolve the disc of Titan, Saturn's largest satellite, and the only satellite in the Solar system to maintain a significant atmosphere (1.5 bars of N_2 mainly and 2% of CH_4). From the ground, Titan can be studied in the near-infrared, where the succession of methane absorption bands and "windows" allows astronomers to study the troposphere and the surface. Indeed, among the plethora of chemical compounds mixed within Titan's atmosphere, methane is the one critical for the visibility of its surface, more efficiently blocking the visible wavelengths than the thick haze layers of aerosols. Nine absorption bands can be found between 0.8 and 5 μm , screening the surface away from Earthling eyes. However, it has been known for some

time now that at precise near-infrared frequencies the methane absorption becomes weak enough to allow astronomers to retrieve information from the surface: these methane windows are centered at 0.83, 1.08, 1.28, 1.6, 2.0, 2.75 and 4.9 μm [e.g., *Griffith et al.*, 1991, 2003; *Lellouch et al.*, 2004; *Coustenis et al.*, 2006]. Besides spectroscopy, images of Titan's resolved disc have been acquired with the Hubble Space Telescope (HST) [*Smith et al.*, 1996; *Meier et al.*, 2000] and with adaptive optics or similar systems [*Gibbard et al.*, 1999; *Brown et al.*, 2002; *Roe et al.*, 2002a, 2002b, 2004; *Bouchez*, 2004; *Bouchez and Brown*, 2005] during the past 10 years. Our own team has been involved in such observations. Following the first Titan data acquired by Adaptive Optics Near-Infrared System (ADONIS) at the European Southern Observatory New Technology Telescope (ESO NTT) [*Combes et al.*, 1997], several more adaptive optics systems were developed and exploited by our team, with among the most recent ones: PUEO (the infrared camera at the Canada France Hawaii Telescope, atop the Mauna Kea, in Hawaii) and Nasmyth Adaptive Optics System Near-Infrared Imager and Spectrograph (NAOS/CONICA) (hereinafter referred to as NACO at the Very Large Telescope (VLT), on Cerro Paranal, Chile; see, for instance, *Rousset et al.* [2003]; *Lenzen et al.* [2003] or <http://www.eso.org/instruments/naco>). Titan's atmosphere and surface have been studied with these systems [*Coustenis*

¹Laboratoire de Planétologie et Géodynamique, Nantes, France.

²Laboratoire d'Etudes Spatiales et d'Instrumentation en Astrophysique, Observatoire de Paris-Meudon, Meudon, France.

³Service d'Aéronomie, Institut Pierre Simon Laplace, Université de Versailles Saint-Quentin-en-Yvelines, Verrières le Buisson, France.

⁴European Southern Observatory, Santiago, Chile.

et al., 2001, 2006; *Gendron et al.*, 2004; *Hartung et al.*, 2004a; *Hirtzig et al.*, 2006].

[3] Apart from the ground-based studies of Titan, an interplanetary probe was launched on 15 October 1997: the orbiter Cassini, carrying the Huygens probe. Cassini arrived in Saturn's system in 2004, and released the Huygens probe on 25 December 2004. The probe entered Titan's atmosphere on 14 January 2005 and safely landed on its surface. Huygens did not need ground-based observations to fulfill its scientific objectives, yet the "ground truth" returned by the probe will only correspond to one single location on Titan's map. Other sources of information were needed at the same time so that these precious measurements could be extrapolated to the entire planet because Cassini in situ observations were not performed during the Huygens mission and in general they are limited in time span. Thus all the Earth-based instruments available, with a time coverage flexibility and powerful instrumentation but a lower spatial resolution, complement the scientific outcome of this mission.

2. Data Acquisition and Processing

[4] We have used NACO to monitor and follow the event of the Huygens descent in Titan's atmosphere and its successful landing. However, we could only observe Titan on 15 and 16 January 2005, hence missing any chance to detect the glow of the probe's entry into the satellite's atmosphere. Huygens landed on Titan's surface on 14 January 2005 at 1138:11 UT [*Lebreton et al.*, 2005], and our run began around 0500 UT on the following day, i.e., 18 hours after the landing itself. Our second night of observation took place between Huygens+41h and Huygens+44h, but the landing site was at that time close to the sub-Earth point (SEP), the center of Titan's disc on our images, which will be particularly useful for our spectroscopic study [see *Negrão et al.*, 2007].

2.1. Observations

[5] We obtained images using the S13 camera (13.25 milliarc seconds (mas)/pixel) with narrowband (NB) and intermediate-band (IB) filters in J and K band. All IB filters have a full width at half maximum (FWHM) bandwidth of 60 nm; for the NB filters the FWHM bandwidth is marked in brackets. We used the filters NB_1.28 (14 nm), IB_2.00, NB_2.12 (22 nm), IB_2.15, and NB_2.17 (23 nm) to probe different altitude levels from the surface to the stratosphere. An approximate Strehl ratio of 10% was achieved with the NB_1.28 filter, and approximately 52% with the filters in K band.

[6] Furthermore, we observed Titan with the Simultaneous Differential Imager (SDI) and the Fabry-Perot (FP) interferometer. The SDI [*Lenzen et al.*, 2004] splits the beam with a double Wollaston prism and allows to register four simultaneous images at 3 wavelengths sampling the methane window at 1.575, 1.600 (both inside the window), and 1.626 μm (outside the window). The filter width is 25 nm (FWHM), and the spatial resolution is 17.3 mas/pixel.

[7] The FP [*Hartung et al.*, 2004b] can be tuned from 2.0 to 2.5 μm with a bandwidth of 2 nm, and spectral resolution of 1100. Since only a small part of the field of view (FOV) is used, no phase map correction has to be

applied, and the FP can be considered as a tunable filter. To keep the exposure times small, we used the S27 camera (27.1 mas/pixel), i.e., half the resolution of the S13 camera. At this pixel scale the image is still Nyquist sampled in K band (whereas the S13 camera oversamples by a factor of 2). The FP scan ranged from 2.00 μm to 2.18 μm (see Figure 1 for all wavelength setups), with an exposure time of 60 sec for each frame.

[8] The spectroscopic (long slit) data that were taken during this run with NACO are discussed by *Negrão et al.* [2007]. Partly, they can be compared with the FP data.

[9] Table 1 lists our observations of Titan in the days following the arrival of the Huygens probe onto the surface of the satellite. At that time, Titan was 0.88 arc sec in diameter, imaged by the VLT with approximately 17 resolution elements in diameter corresponding to 300-km spatial resolution under optimal conditions. The AO correction was optimal thanks to the good average seeing ranging from 0.4" to 0.6". The regions and features probed by spectroscopy could be studied with precision, and high contrast and signal-to-noise ratio were achieved.

[10] Table 1 shows the filters we used, covering several of the methane windows. The intermediate and narrowband filters IB_2.00, NB_2.12, IB_2.15 and NB_2.17, together with the FP scan, cover the 2.0 μm window and its upper wing. The H band is covered by the SDI instrument, returning simultaneous images of the center and wings of the 1.6 μm window: the surface of Titan is reached at 1.575 and 1.600 μm , while the atmosphere is studied at 1.625 μm .

[11] The central wavelength of any given filter with respect to the methane bands defines the altitude probed in Titan's atmosphere, as reported in Table 2. Some filters contain both surface and atmosphere contributions (IB_2.00 in particular), and precaution is needed in such cases when trying to separate these contributions.

[12] Figure 1 displays a large sample of our images acquired in January 2005. (These data can also be found on our Web site http://www.lesia.obspm.fr/planeto/Titan/Titan_sol_ao/Index.html.) Some wavelengths appear several times, for different reasons. Figure 1 (top) shows the SDI and NB images acquired on 16 January, and Figure 1 (bottom) presents the FP images on 15 January. The SDI mode returns two images at 1.62 μm , through two different optical systems. This is a good test of our processing methods: we will keep one image for each path ("a" or "b") until the final steps. Among the narrowband data are also two images at 2.12 μm , sorted chronologically from left to right. At this wavelength, where the bright south polar feature usually appears, we acquired images at two consecutive nights, so that we could monitor the short-term evolution of this phenomenon (see the observing log in Table 1).

[13] With the SDI a spatial resolution of 60 mas is obtained, reaching the diffraction limit after deconvolution (see hereafter). The pixel scale for the FP images is 27 mas/pixel. The resolution of the deconvolved images is better than 70 mas which is close to the diffraction limit.

2.2. Data Processing

[14] The processing applied to the data is identical to the one described by *Combes et al.* [1997], *Coustenis et al.*

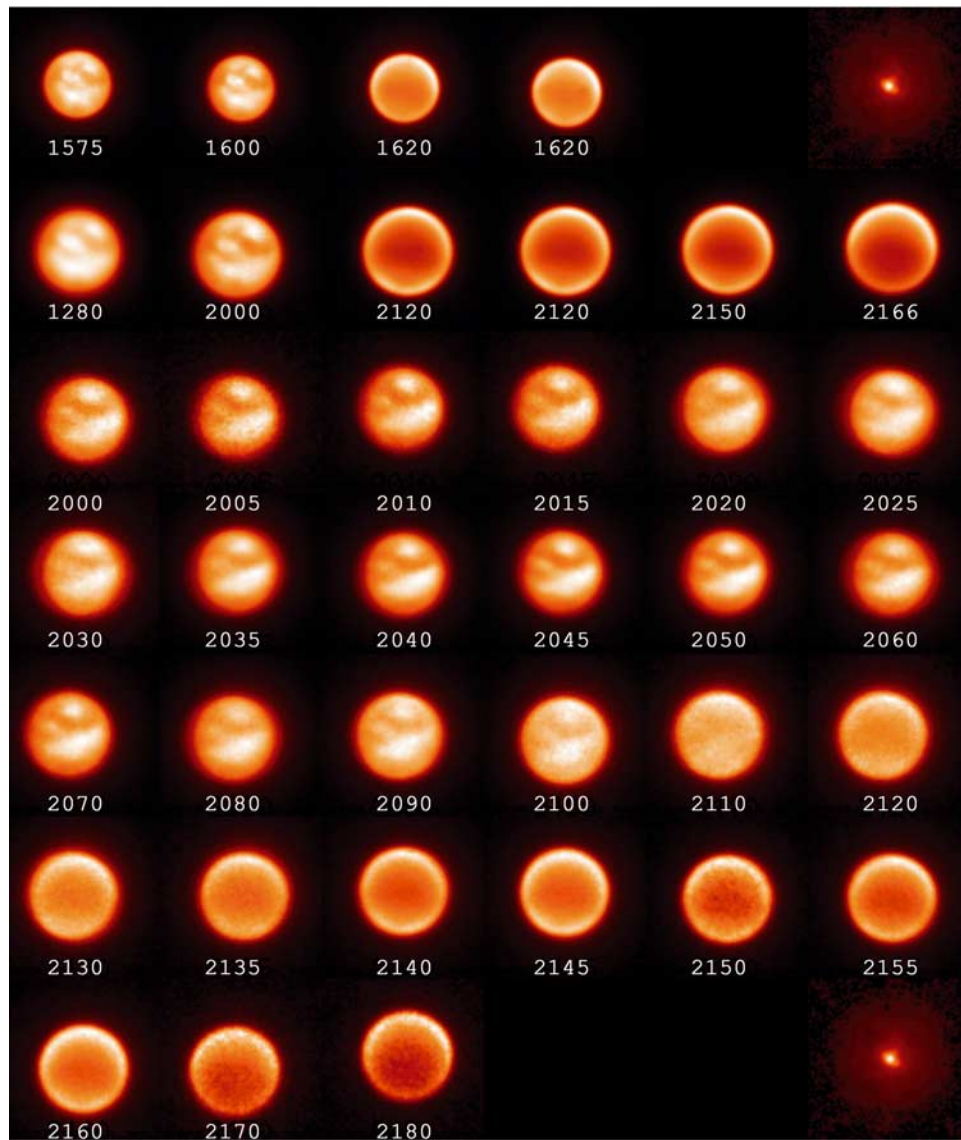


Figure 1. NACO images (nondeconvolved) of Titan acquired in January 2005. These images are only treated for bad pixels and flat field effects. They are sorted by instrument mode and by increasing probed altitude (the corresponding wavelength is given in angstroms). From top to bottom, we show the SDI (16 January), NB (16 January), and FP (15 January) images. A $2.0 \mu\text{m}$ PSF is also given for the narrowband and SDI images and another one for the FP data.

[2001], or *Coustenis et al.* [2006] for the regular imagery data. The NB filter images, the FP and the SDI data are first flat fielded, and then treated for any remaining bad pixels. The last step of the process is eventually deconvolution, generally applying the Magain method [*Magain et al.*, 1998], where we use photometric standard star images as point spread function (PSF) references to enhance the contrast of the images. Because of a coarser pixel size in the case of the FP data, we used the *Bratsolis and Sigelle* [2001] version of the Richardson-Lucy deconvolution method, reaching a final resolution of better than 70 mas. The Magain method did not converge correctly in those cases (because of the low signal-to-noise ratio (SNR) of some of the FP images, in particular longward of $2.17 \mu\text{m}$ as can be seen on Figure 1). For coherence reasons and also in order to ensure the validity of any comparison between

all the images from this series, we therefore had to select the only deconvolution method which allows us to process all the FP data, namely, the Richardson-Lucy (RL) inspired Bratsolis method. Figure 2 shows the effect of the deconvolution processes on our images with the enhancement of the present features.

[15] The FP data require further processing, in particular to precisely determine the wavelength used for each position. The tuning of the instrument during the night of observations and the resulting processing steps will be explained in detail by *Hartung et al.* [2007]; another FP data set related to trace solid CO_2 ice on Titan's surface is described by *Hartung et al.* [2006].

[16] Studying the surface or the atmosphere of Titan may require additional processing. If we focus on the surface of Titan, as done by *Coustenis et al.* [2006], then we have to

Table 1. Titan Adaptive Optics Observations in January 2005 With VLT/NACO^a

Time, UT	Filter	Experiment Time, s	Seeing
<i>15 January 2005^b</i>			
0522	SDI	5.0	0.6–1.2
0623	FP	60.0	
<i>16 January 2005^c</i>			
0340	IB_2.00	60.0	0.4–1.4
	NB_2.12	100.0	
	IB_2.15	60.0	
	NB_2.17	60.0	
	NB_2.18	20.0	
0532	SDI	5.0	0.60
	S27_3_SK	240.0	
0630	S27_3_SK	240.0	0.60
0700	S27_3_SK	240.0	0.60

^aSeeing values given are either average values for stable seeings (i.e., ± 0.1) or the range of values during the observation.

^bTitan: 7 hours, 43 min, 40 s; $+21^{\circ}21'24''$; SEP, 22° S, $170-172^{\circ}$ LCM; phase, $+0.12^{\circ}$; PSF, HD 60 778, A1V at $M_V = 9.12$ [Perryman et al., 1997].

^cTitan: 7 hours, 42 min, 20 s; $+21^{\circ}22'21''$; SEP, 22° S, $192-194^{\circ}$ LCM; phase, $+0.25^{\circ}$; PSF, Hip058454, G0V at $M_V = 8.40$ [Perryman et al., 1997]; HD 60 778, A1V at $M_V = 9.12$ [Perryman et al., 1997].

eliminate the atmospheric contribution from the images, and correct for center-to-limb effects. The former is done by subtracting the flux recorded on atmosphere-only images (for instance the $1.620 \mu\text{m}$ SDI image for the H band, or the IB_2.15 data in K band). One problem can arise when the width of the surface filter and the atmosphere filter used as reference do not overlap. It is the case for all the FP images. When the filters do not overlap, we cannot ensure that the atmospheric contribution will be the same in both images, thus limiting the accuracy of the correction. This will lead to $\approx 10\%$ error bars in absolute flux on the limb where the correction of the atmosphere is obviously the strongest. Yet this effect is negligible if we consider only regions within 60° from the center of the disc of Titan.

[17] The correction for the center-to-limb effects is done by applying a cylindrical filter produced by our radiative transfer model (see below). The flux is corrected to recover a geometry-free image of Titan's surface, given the angles of incidence and emission of the light, as can be found in the Institut de Mécanique Céleste et de Calcul des Ephémérides (<http://www.imcce.fr/imcce.php>) tables.

Table 2. NACO Filters Used for the Observations in 2005^a

Filter	$\lambda \mu\text{m}$	Altitude Probed						Surface		
		Nadir			Limb			T^2	C	
		min	nom	max	min	nom	max			
SDI	1.575 ± 0.012	0.0	0.0	0.0	8.8	8.9	9.0	++	53.3	89.6
	1.600 ± 0.012	0.0	0.5	10.4	9.2	13.0	104.2	++	33.4	79.7
	1.620 ± 0.012	0.0	33.2	210.7	15.8	58.2	249.8		00.2	06.8
NB_1.28	$1,282 \pm 0,007$	0	0	0	2.0	2.9	3.6	++	59.4	82.6
IB_2.00	2.000 ± 0.030	0.0	3.8	111.4	9.1	15.9	157.4	++	47.6	79.4
NB_2.12	2.120 ± 0.010	0.0	0.0	0.0	17.3	18.4	23.8		19.7	82.9
IB_2.15	2.150 ± 0.030	1.0	35.0	278.1	18.7	56.6	314.7		00.3	11.4
NB_2.17	2.166 ± 0.010	25.8	72.2	323.7	39.7	96.0	359.0		00.0	00.0
FP	2.000 ± 0.001	0.0	0.1	0.0	9.3	9.6	9.4	++	55.3	92.3
	2.005 ± 0.001	0.0	2.1	0.0	9.2	12.6	15.8	++	55.5	91.3
	2.010 ± 0.001	0.0	0.0	0.0	9.2	10.0	22.9	++	58.8	93.3
	2.015 ± 0.001	0.0	0.0	0.0	9.1	9.2	9.2	++	67.7	94.4
	2.020 ± 0.001	0.0	0.0	0.0	9.1	9.1	9.1	++	69.2	94.5
	2.025 ± 0.001	0.0	0.0	0.0	9.1	9.2	9.3	++	67.1	94.4
	2.030 ± 0.001	0.0	0.0	0.0	9.1	9.2	9.2	++	68.2	94.5
	2.035 ± 0.001	0.0	0.0	0.0	9.1	9.2	9.2	++	68.2	94.5
	2.040 ± 0.001	0.0	0.0	0.0	9.1	9.2	9.2	++	69.0	94.6
	2.045 ± 0.001	0.0	0.0	0.0	9.2	9.2	9.2	++	69.9	94.6
	2.050 ± 0.001	0.0	0.0	0.0	9.2	9.2	9.2	++	68.7	94.6
	2.060 ± 0.001	0.0	0.0	0.0	9.3	9.3	9.3	++	62.2	94.1
	2.070 ± 0.001	0.0	0.0	0.0	9.3	9.4	9.4	++	59.1	93.8
	2.080 ± 0.001	0.0	0.0	0.0	9.4	9.4	9.4	++	55.8	93.5
	2.090 ± 0.001	0.0	0.0	0.0	9.4	9.4	9.4	+	50.7	92.9
	2.100 ± 0.001	0.0	0.0	0.0	11.7	12.0	12.4	+	43.4	91.7
	2.110 ± 0.001	0.0	0.0	0.0	15.7	15.9	16.1	+	31.3	88.7
	2.120 ± 0.001	0.0	0.0	0.0	18.2	18.7	22.9		17.1	80.9
2.130 ± 0.001	0.0	0.2	0.0	18.3	19.3	20.4		15.0	78.6	
2.135 ± 0.001	0.0	4.7	19.1	18.5	26.7	73.3		05.2	51.5	
2.140 ± 0.001	1.3	5.3	41.4	18.8	24.5	100.2		04.6	51.0	
2.145 ± 0.001	6.4	7.5	7.2	22.0	24.2	24.0		01.1	22.4	
2.150 ± 0.001	14.5	34.6	101.6	27.7	56.6	148.9		00.0	00.0	
2.155 ± 0.001	34.6	77.1	278.1	50.1	99.6	314.7		00.0	00.0	
2.160 ± 0.001	25.9	37.4	66.5	39.8	59.1	101.5		00.0	00.0	
2.170 ± 0.001	42.9	81.1	210.3	58.1	103.8	249.5		00.0	00.0	
2.180 ± 0.001	46.9	65.5	139.8	59.3	80.4	166.4		00.0	00.0	

^aEach filter is described by its wavelength and width, which defines the range of altitudes probed. Six altitudes are given: three at the limb and three at the center of Titan's disc. The nominal altitude (nom) corresponds to the maximum of the contribution function; the minimum (min) and maximum (max) altitudes correspond to values reached within the spectral width of the filters. Finally, the surface contribution is summarized: first qualitatively (the more pluses, the clearer the surface signal) and then quantitatively by the values of two-way transmission T^2 and contrast C .

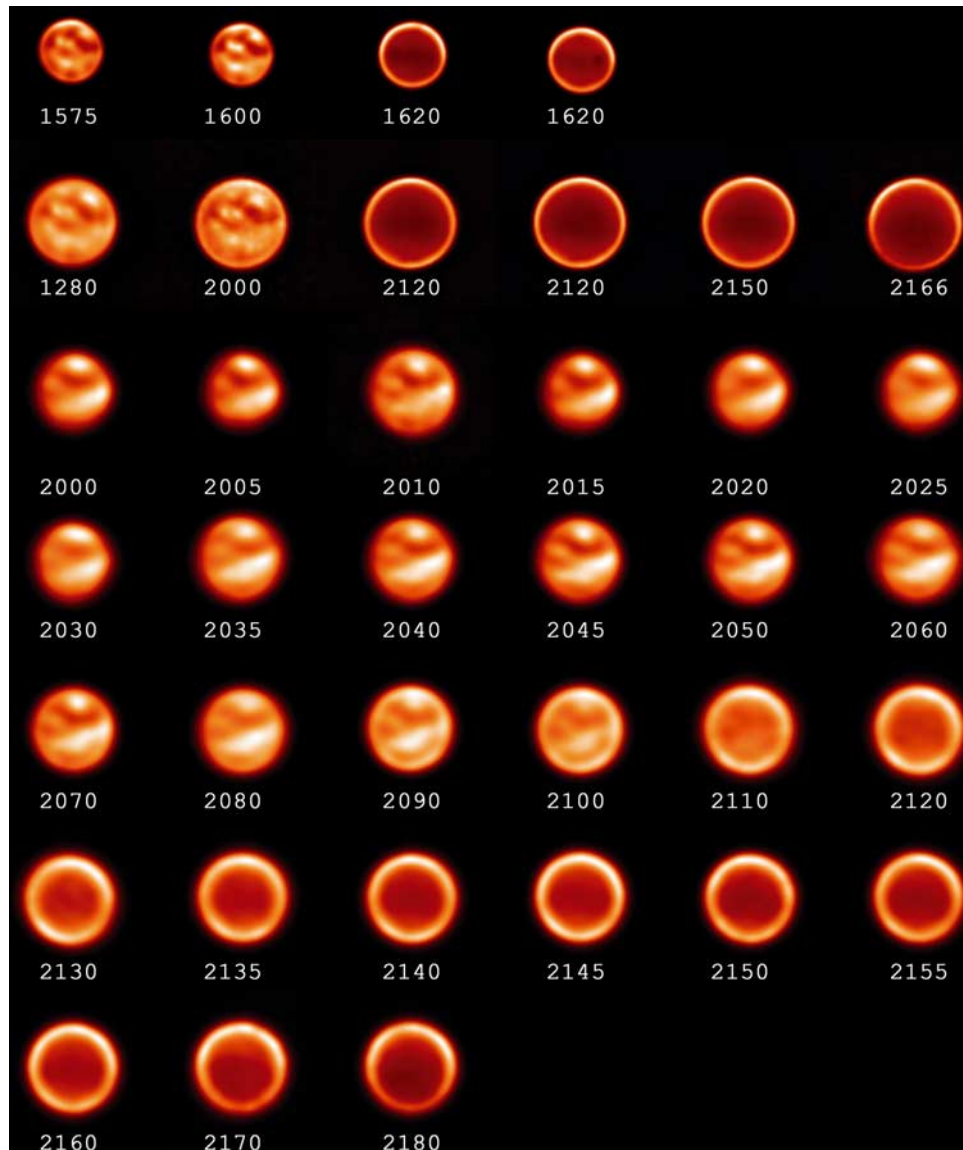


Figure 2. Deconvolved images of Titan. These images correspond exactly to the ones selected on Figure 1, but they now reach the diffraction limit thanks to the Magain deconvolution (or only four times the diffraction limit with the RL-Bratsolis method in the case of the low SNR FP images).

[18] On the other hand, we do not correct for those two effects when studying the atmospheric phenomena. The application of the center-to-limb correction is too sensitive to errors of locating of Titan's disc center. Indeed, any Minnaert or Lambert law will have the corrected flux diverge on the limbs (and our theoretical curve returned by the model is no exception): if a cylindrical mask is shifted by even only one pixel from the real position of Titan's disc center, then the flux variation on the limb can easily reach 40%. Yet the measured flux on the undeconvolved images is not nil, because the atmosphere extends far into space. Therefore we consider only a one-resolution-element-thick group of pixels on the disc limb (from about 70 to 90° from the nadir) as read on the deconvolved images. These pixels will be used for relative comparison, and not for absolute measurements, as done by *Hirtzig et al.* [2006].

[19] In brief, we follow two procedures: (1) For atmospheric diagnostics (see Figures 3 and 4), we do not process further than absolutely required the deconvolved images, but we restrain our selection of data onto the limb of Titan for relative measurements exclusively, and (2) for surface studies (see Figure 5), we try to cancel the atmospheric contribution and correct for the center-to-limb effects by modeling, leading to 10% error bars on the absolute flux.

2.3. Radiative Transfer Model

[20] In studies of either the atmosphere or the surface of a planet, a complete radiative transfer model is compulsory. It will be used in the former case to compute the altitude probed by the filters, or in the latter case to simulate the atmospheric response, the geometry effects and retrieve the surface albedo value from the measured geometrical albedo.



Figure 3. Selection of deconvolved atmosphere images, sorted by increasing altitude (15, 19, 22, 47 and 79 km, respectively). The north-south asymmetry shows a bright northern limb, with contrasts increasing when probing higher altitudes.

[21] We use the microphysical and radiative transfer code of *Rannou et al.* [2003]. This is an updated version of the one described by *McKay et al.* [1989] but uses fractal shaped aerosols instead. All the parameters and the sensitivity of the model to them are fully described by *Rannou et al.* [2003]. Some parameter values were updated based on a

work applied specifically to Titan 3- μm spectra from the Infrared Space Observatory [*Coustenis et al.*, 2006] and ground-based near-infrared measurements from 1 to 2.5 μm [*Negrão et al.*, 2006]. There were improvements in the haze vertical profile, methane abundance and methane coefficients. A geometrical correction was also implemented to

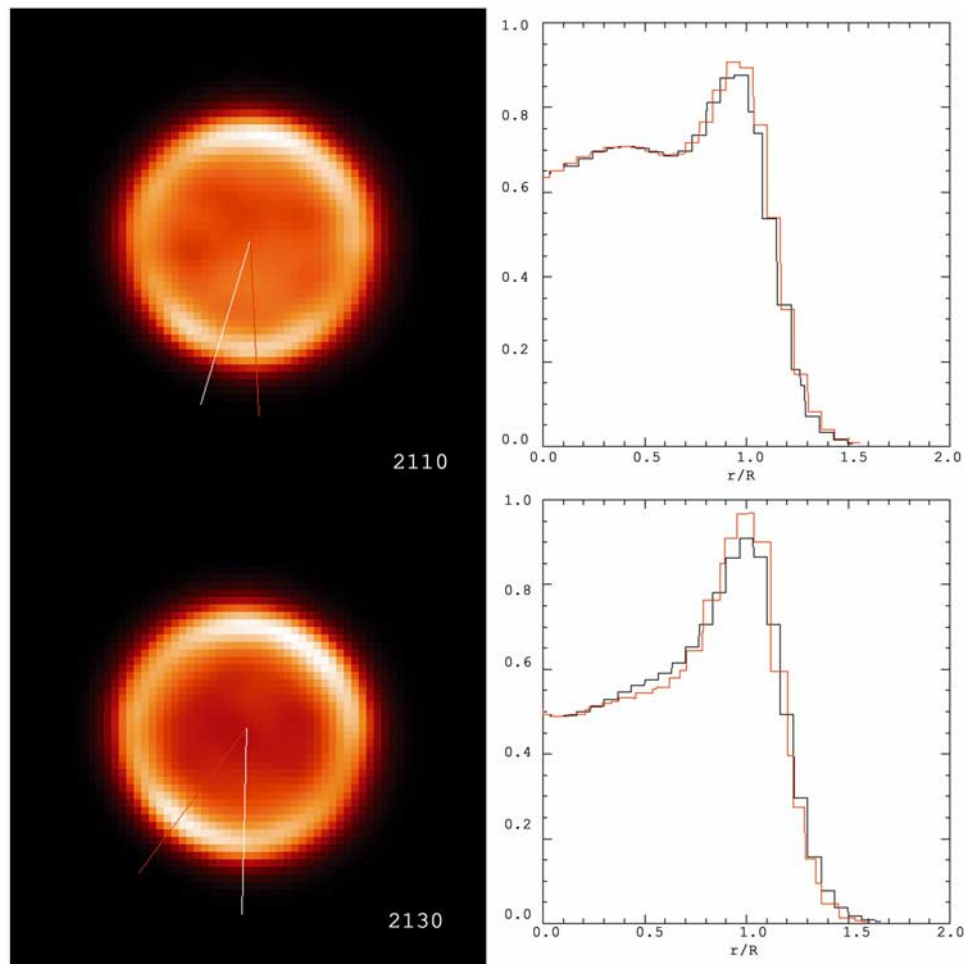


Figure 4. Hints for a disappearing bright south polar feature apparent since 1999. (top left) Deconvolved 2.12 μm image acquired with the NB mode of NACO, and two intensity profiles (in arbitrary units normalized with respect to the brightest pixel in the image) from the center of Titan's disc to the limb, one passing above the south pole (in orange), and the other cutting through the surrounding limb (black). (bottom left) Deconvolved FP 2.130 μm image and two profiles extracted from it (through the bright feature on the southwest limb in red, and through the average southern limb in black). The large meteorological system detected since 1999 [*Bouchez and Brown*, 2005; *Gibbard et al.*, 2004; *Hirtzig et al.*, 2006; *Roe et al.*, 2002b, 2005, and references therein] and confirmed by Cassini in 2004 [*Porco et al.*, 2005] is now barely visible, at most 10% brighter than the surrounding areas; yet a western companion [*Hirtzig et al.*, 2006] is still visible, 87% brighter than the dark areas.

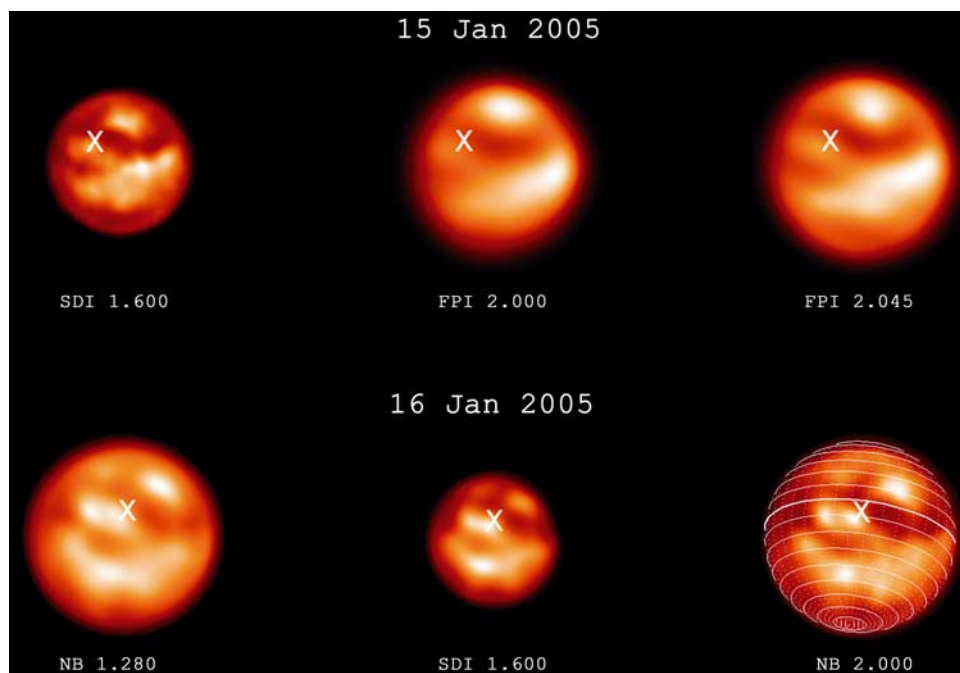


Figure 5. Sample of deconvolved surface images, cleaned of the atmosphere contribution, in the H and K bands. (top) A selection of SDI and FP images from 15 January, and (bottom) views acquired with the NB and SDI filters on 16 January 2005. A coordinate system is superimposed onto the last NB image. The trailing side of Titan shows the same succession of bright and dark patches, probably somehow related to topography, regardless of the wavelength chosen. The Huygens landing site is close to the center of the disc (-10°S , 192° Longitude of Central Meridian (LCM)).

better take into account the intensity near the limb. We refer the reader to *Coustenis et al.* [2006] for more details.

[22] The model computed three altitudes per filter for two different zenith-observer angles. Photons at one given wavelength will probe from the top of the atmosphere to a specific $\tau_{\text{eff}} = 1$ level (τ_{eff} is the effective opacity which, contrary to the ‘normal’ opacity, takes into account the photons forward scattered by the haze [see *Rannou et al.*, 2003; *Pollack and McKay*, 1985]). Since methane absorption coefficients can vary significantly within each filter, in Table 2 we report three different altitudes: the minimum and maximum values correspond to the range of $\tau_{\text{eff}} = 1$ level altitudes found over the FWHM of the filter considered, while the nominal value returns the weighted average of these altitudes over the bandwidth of the filter. The former range often overlaps the altitude range where the contribution is high, meaning most of the photons received will originate from this layer.

[23] Together with the maximum, minimum and average altitudes, we also show, in Table 2, the calculated values of total transmission T^2 and contrast C . The former returns the percentage of solar photons reaching the surface then bouncing back to us (for a theoretical surface albedo of 1.0), and the latter is defined as

$$C = [ga(sa = 1) - ga(sa = 0)] / [ga(sa = 1) + ga(sa = 0)]$$

where $ga(sa = 1)$ and $ga(sa = 0)$ refer to the geometric albedo calculated using a surface albedo equal to 1 and 0,

respectively. Contrary to the transmission, the contrast gives a measure of the number of photons which arrive to the last atmospheric layer considered either directly (as transmission) or diffused. These two parameters, together with the altitude values will help later on to constrain and identify if a certain feature is a surface or an atmospheric one.

[24] We have considered the uncertainty on the methane absorption and distribution as well as on the aerosol distribution. The impact of the methane concentration at the surface ($5 \pm 2\%$) led to small error bars on the altitude ranges (at most 1 km variations), and to some uncertainty on the T^2 and C : the sensitivity to the methane concentration is highest in the wings of the methane absorption bands, with absolute error bars reaching 10–12% (from 2.12 to 2.15 μm), and only 1–3% in the cores of the methane windows and bands. We also computed variations on the aerosol profiles (by adding or subtracting 10% of the haze concentration) and used the methane absorption coefficients from the band model by *Irwin et al.* [2006] (for details, see *Negrão et al.* [2007]). This finally leads to an absolute uncertainty of nearly 15% in the wings of the methane bands. Therefore, at 2.11 μm , T^2 reaches $31 \pm 15\%$, and $17 \pm 15\%$ at 2.12 μm . Given these uncertainties, we cannot claim we receive any photons from the surface longward of 2.12 μm . Even beyond 2.10 μm , the transmission is lower than 50%, and, although we do detect a surface signal (see Figure 5) at such wavelengths, any deductions on surface properties are to be taken with caution.

[25] Table 2 summarizes all the altitudes we could probe down to the surface sorted by instrument and filter. The FP

provides the smallest bandpass probing layers only a few kilometers thick.

3. Diagnostic of Titan's Atmosphere

[26] Some of the data we present here are also part of the study published by *Hirtzig et al.* [2006] devoted to a long-term coverage of Titan, using intermediate-band (IB) and narrowband (NB) filters. This was done so as to complete the monitoring of atmospheric phenomena that we have been pursuing since 1998. Here we present a more focused study of the NB, SDI and FP data taken during the two days following the Huygens probe descent in Titan's atmosphere so as to provide all associated information that can be extracted from our images and could be relevant to this space mission significant achievement.

[27] Figure 3 shows samples of the atmospheric images we acquired on 15 and 16 January 2005, featuring essentially the predominating north-south asymmetry but also antiphase or diurnal effects (hints for a nocturnal condensation of stratospheric aerosols [*Coustenis et al.*, 2001; *Hirtzig et al.*, 2006]).

3.1. North-South Asymmetry

[28] The north-south asymmetry of Titan has been investigated since the 80s, when Voyager detected an excess of aerosols in the northern (winter) hemisphere. This situation was manifested by a bright southern limb in the visible (due to a relative excess of methane in the southern hemisphere, inducing more Rayleigh diffusion), or a bright northern limb in the infrared (which is analogous but instead involves diffusion by fractal aerosol aggregates).

[29] In the 90s, the situation had reversed, with a bright southern limb (or "Titan's smile"), detected by both the HST [*Caldwell et al.*, 1992; *Smith et al.*, 1996] and several adaptive optics, speckle or tip tilt systems [*Combes et al.*, 1997; *Gibbard et al.*, 1999]. In 1996, the season had advanced on Titan, and again a new reversal of this north-south asymmetry could be detected first in the visible by the HST [*Lorenz et al.*, 1999]. This inversion (with the north pole brighter in the near-IR) was found in infrared images starting from 2002 [*Hirtzig et al.*, 2006] approximately, while the reversal was propagating to lower and lower altitudes as time went by, mainly because the higher altitudes are more sensitive to the changes in solar flux. This last reversal led to the current situation: a bright northern limb at every wavelength, as visible on Figure 3. We will focus here on a diagnostic of the north-south asymmetry, as a function of altitude, at the time of the probe descent to better constrain the atmospheric component in all studies related to Huygens. It is possible to extract such information from the FP data, since the probed altitude can be fine tuned.

[30] Table 3 lists all the measurements of the north-south limb ratios. This ratio is determined by comparing the flux of the uppermost northern resolution element placed on Titan's limb to the flux from the southernmost resolution element. The use of deconvolved images does not change the conclusion drawn (i.e., the northern limb is the brightest at all wavelengths), even though photometry is not conserved, it simply demonstrates that the deconvolution

enhances the features already present, allowing for a better SNR and smaller error bars.

3.2. Stratospheric Haze Enhancement

[31] Phase effects are always important in the appearance of Titan's eastern and western limbs, but *Coustenis et al.* [2001] first detected an additional effect in 1998, identified as a diurnal effect with a morningside haze enhancement, and confirmed with the NB images taken since and in particular in 2005 [*Hirtzig et al.*, 2006]. We will focus here on the eventual signatures for this phenomenon in the various sources at our disposal.

[32] At the time of Huygens landing, the solar phase angle value ($+0.12^\circ$ on 15 January) induces a brighter eastern (evening) limb. Yet in cases of small positive phase angles (as was the case in January 2005 shortly after Saturn's opposition), the brightest limb is on the contrary the western (morning) one. This is obvious for instance on the NB images presented Figure 3. This phenomenon is interpreted [*Coustenis et al.*, 2001] as the signature of stratospheric aerosols having condensed during Titan's night and appearing on the morning limb as they disaggregate in the solar dawn.

[33] Similar to Table 3, we compute here ratios of the eastern/western limbs by drawing latitudinal profiles of intensity. The error bars originate in the flux variation within the resolution element considered; the nominal value is computed from the average value over this resolution element. The font used in Table 4 underlines visually the meaning of each data point: the regular font corresponds to a regular phase effect, as should be expected given the sign of the solar phase angle (i.e., a phase effect on the eastern limb in mid-January 2005); bold faces underline an anti-phase effect, signature of this diurnal phenomenon of nocturnal aerosols condensation; finally, lines in italics indicate results that cannot be used to infirm or confirm any hypothesis, because both limbs are identically bright within our error bars.

[34] First, we note that the regular phase effect is only apparent in a few cases: the surface SDI images on 16 January show this phenomenon. This could also be due to or enhanced by the surface contribution appearing in our images as bright surface features approaching the eastern limb on 16 January (Figure 5). The low SNR of the undeconvolved images also leads to uncertainties on the observed features (the majority of the measurements from "raw" images is displayed in italics, underlining that both limbs are of similar intensity). The use of deconvolution methods allows us to enhance the low-frequency signal already present in the Fourier Transform of the "raw" data, and to recover more spatially delimited features.

[35] On the other hand, when including all filters, there are 8 firm detections out of 20, with 13 unclear situations for the FP data. This tends to prove that we are in presence of a statistically sound phenomenon. The effect is larger at higher altitudes (NB_2.17 in particular). Finally, the FP data, whose expected high precision was promising, are somehow disappointing. Because we did not achieve good results with more precise deconvolution methods, we have not recovered a high spatial resolution, inducing large-sized resolution elements, and hence large variations of flux within the resolution elements, meaning large error bars.

Table 3. Ratios of the LIMB Fluxes N/S, Characteristic of the Contrast of the North-South Asymmetry^a

Filter	λ , μm	Altitude Limb		N/S Ratio			
		min, km	max, km	15 January 2005		16 January 2005	
				Raw	Dec	Raw	Dec
SDI	1.575	8.3	8.4	1.180 ± 0.133	1.273 ± 0.025	1.201 ± 0.038	1.387 ± 0.009
	1.600	9.1	140	1.140 ± 0.104	1.344 ± 0.060	1.179 ± 0.047	1.231 ± 0.036
a	1.620	18	221	1.178 ± 0.066	1.281 ± 0.055	1.141 ± 0.066	1.608 ± 0.052
b	1.620	18	221	1.139 ± 0.066	1.386 ± 0.045	1.198 ± 0.081	1.569 ± 0.066
IB_2.00	2.000	9	201	-	-	1.280 ± 0.409	1.328 ± 0.012
NB_2.12	2.120	17	23	-	-	1.168 ± 0.024	1.216 ± 0.023
IB_2.15	2.150	19	214	-	-	1.230 ± 0.014	1.350 ± 0.012
NB_2.17	2.166	40	311	-	-	1.511 ± 0.064	1.653 ± 0.027
FP	2.090	9.4	9.4	1.175 ± 0.065	1.220 ± 0.071	-	-
	2.100	10.8	11.5	1.011 ± 0.051	1.146 ± 0.039	-	-
	2.110	15	16	1.134 ± 0.103	1.103 ± 0.026	-	-
	2.120	18	23	1.170 ± 0.111	1.099 ± 0.023	-	-
	2.130	18	19	1.158 ± 0.056	1.057 ± 0.054	-	-
	2.135	18	21	1.195 ± 0.070	1.137 ± 0.043	-	-
	2.140	20	25	1.123 ± 0.097	1.130 ± 0.052	-	-
	2.145	22	24	1.082 ± 0.071	1.110 ± 0.015	-	-
	2.150	29	83	1.156 ± 0.101	1.216 ± 0.071	-	-
	2.155	62	315	1.169 ± 0.054	1.183 ± 0.044	-	-
	2.160	45	101	1.132 ± 0.298	1.184 ± 0.026	-	-
	2.170	58	250	1.583 ± 0.359	1.588 ± 0.090	-	-
	2.180	60	138	1.499 ± 0.185	1.586 ± 0.046	-	-

^aThis parameter is studied for both undeconvolved (Raw) and deconvolved (Dec) images. The altitude probed by each filter is also reported here for clarity. Images where the surface contribution is predominant are not used here. As described in section 2.1, the SDI provides four beams that probe simultaneously atmosphere and surface at 1.575, 1.600, and 1.620 μm . The two filters with the same wavelengths 1.625 μm are distinguished by a and b.

The nominal values tend to confirm that the western limb is the brightest above 20 km of altitude, but the SNR is too low to confirm this trend.

3.3. Clouds and the Polar South Feature

[36] To date there have been reports on several detections of clouds on Titan, either deduced from spectroscopy

[Griffith *et al.*, 1998] or observed directly by adaptive optics, the HST or the Cassini-Huygens mission. Four different features were distinguished, but their names vary from team to team, and their altitudes and natures are extremely model-dependent, and thus still puzzling.

[37] 1. A serpentine feature in the low stratosphere [Hirtzig *et al.*, 2006], or “polar collar” [Roe *et al.*,

Table 4. List of the E/W Fluxes Ratios^a

Filter	λ , μm	Altitude Limb		E/W Ratio			
		min, km	max, km	15 January 2005 (+0.12°)		16 January 2005 (+0.25°)	
				Raw	Dec	Raw	Dec
SDI	1.575	8.3	8.4	1.025 ± 0.142	0.901 ± 0.068	0.916 ± 0.132	1.092 ± 0.033
	1.600	9.1	140	1.003 ± 0.224	0.950 ± 0.054	0.919 ± 0.126	1.333 ± 0.085
a	1.620	18	221	0.991 ± 0.131	0.960 ± 0.090	0.952 ± 0.087	0.908 ± 0.039
b	1.620	18	221	0.895 ± 0.073	0.913 ± 0.037	0.976 ± 0.069	0.875 ± 0.033
NB_2.12	2.120	17	23	-	-	1.007 ± 0.140	0.964 ± 0.023
IB_2.15	2.150	19	214	-	-	0.987 ± 0.142	0.940 ± 0.044
NB_2.17	2.166	40	311	-	-	1.006 ± 0.146	0.815 ± 0.037
FP	2.090	9.4	9.4	1.000 ± 0.875	1.015 ± 0.322	-	-
	2.100	10.8	11.5	1.018 ± 0.891	1.026 ± 0.230	-	-
	2.110	15	16	1.054 ± 0.090	1.007 ± 0.152	-	-
	2.120	18	23	0.989 ± 0.271	0.937 ± 0.200	-	-
	2.130	18	19	0.982 ± 0.177	0.908 ± 0.135	-	-
	2.135	19	21	0.962 ± 0.150	0.956 ± 0.202	-	-
	2.140	20	25	0.980 ± 0.264	0.923 ± 0.113	-	-
	2.145	22	24	0.976 ± 0.108	0.926 ± 0.209	-	-
	2.150	29	83	0.971 ± 0.187	0.905 ± 0.175	-	-
	2.155	62	315	0.988 ± 0.177	0.918 ± 0.181	-	-
	2.160	45	101	0.986 ± 0.359	0.925 ± 0.182	-	-
	2.170	58	250	0.942 ± 0.065	0.885 ± 0.16	-	-
	2.180	60	138	1.001 ± 0.213	0.915 ± 0.146	-	-

^aAs measured on either undeconvolved (Raw) or deconvolved (Dec) atmosphere images taken in January 2005. Bold values correspond to “antiphase observations” underlining a strong limb brightening opposite to the phase effect prediction (understood as a signature of the “stratospheric haze enhancement”). Italic values correspond to cases where both the eastern and western limbs are similarly bright (their fluxes are equal within the error bars).

2002b], perhaps involving a polar cap of haze, as predicted by the general circulation models (GCMs). The “tropopause cirrus” detected indirectly by *Brown et al.* [2002], lies at a different altitude (40 km instead of 100 km), but it might also be somehow related to this phenomenon.

[38] 2. “Zonal streaks” detected by visual and infrared mapping spectrometer (VIMS) [*Griffith et al.*, 2005] and similar features were observed by International Space Station (ISS) [*Porco et al.*, 2005].

[39] 3. “Transient clouds”, observed by many teams, distributed at southern latitudes, as in *Brown et al.* [2002]; *Roe et al.* [2002a]; *Bouchez* [2004]; *Gibbard et al.* [2003]; *Bouchez and Brown* [2005]; *Porco et al.* [2005], or at midlatitudes [*Roe et al.*, 2005].

[40] 4. A “field of small clouds” [*Porco et al.*, 2005], detected regularly since 2000 [*Brown et al.*, 2002; *Roe et al.*, 2002a; *Bouchez*, 2004; *Gibbard et al.*, 2003; *Schaller et al.*, 2004; *Bouchez and Brown*, 2005; *Porco et al.*, 2005; *Hirtzig et al.*, 2006], resolved only with the Cassini instruments, but that can be seen as a large polar feature hovering above Titan’s south pole, and that we will call from now on “South Polar Feature” (SPF).

[41] Among all these phenomena, we focus here only on the latter, the SPF, which is the only one that we could observe. After some 5 years of intense activity, (having first appeared in 1999 and visible in particular at 2.12 μm), it seems that this large (≈ 1000 km wide) system is vanishing since January 2005. Our group has tracked this feature and reported it since the beginning, along with other investigators (H. G. Roe, S. G. Gibbard, and so on).

[42] Figure 4 summarizes our most recent data regarding the SPF [*Hirtzig et al.*, 2006; *Schaller et al.*, 2004]. While a bright spot (sometimes as much as 300% brighter than its surroundings) was obvious on all the 2.12 μm images from 2001 to 2004, in January 2005 we can hardly see it any more. At 2.12 μm , a feeble feature is visible, less than 10% brighter than the limb it is contained within. On the FP image at 2.11 μm , it is 6% brighter than the limb (and 28% brighter than the dark area close to the limb). Yet the error bar on the flux value within one resolution element, inherent to the very definition of a resolution element (better than 70 mas), reaches about 10% also. We thus cannot ascertain the existence of any such cloud at the time of Huygens’ descent.

[43] Yet at other wavelengths, as was already visible on Figure 2, and underlined on Figure 4, some other atmospheric phenomena are still visible near the south pole. In particular, we detect on the southwest limb a bright elongated feature remindful of a companion of the so-called south polar feature, as described by *Hirtzig et al.* [2006]. The regular large cloud was often paired with two unmoving companions on each side of the limb. Here we only detect the western one, on the morning side, at 60–70°S. It is 11–15% brighter than the limb close to it, and 87% brighter than the dark region close to the center of the disc. These two companions are supposed to be the signature of a remnant stratospheric hood of haze swept away from the Equator, as predicted by the dynamical models of the atmosphere. This may be related also to the “tropopause cirrus” of *Brown et al.* [2002]. On the other hand, they could be clouds or some such other phenomenon, on their own account. The question (to which we cannot offer an

answer now) is why would only the western formation remained visible at that time.

4. Titan’s Surface

[44] Our resulting Titan surface images with all NACO imaging mode are shown in Figure 5 with a spherical projection simulating Titan’s geometry at the time of the observation. As explained briefly in section 2.2, all these final images are processed to eliminate as much of the atmosphere contribution as possible.

[45] Our narrowband filter observations are consistent with previously published surface maps: *Combes et al.* [1997]; *Meier et al.* [2000]; *Roe et al.* [2002a]; *Gendron et al.* [2004]; *Hartung et al.* [2004a]; and *Coustenis et al.* [2006].

[46] The contrast of these bright features is greater at longer wavelengths: the ratio of the intensity of the brightest patch over the intensity of the darkest one reaches 2.0 at 1.28 μm , 2.5 at 1.6 μm , and 2.8 at 2 μm .

[47] The Huygens landing site is clearly visible in our images. This region stands between one bright (to the south) and one dark (to the north) patches, so that there is a high gradient of luminosity. At 2.00 μm , this area is 20–40% darker than the brightest regions over the size of our resolution element (spanning here about 320 km in diameter). We know from the Descent Imager-Spectral Radiometer (DISR) results [*Tomasko et al.*, 2005] that this very region is highly contrasted, in particular on the 70-km large panoramic views acquired by the cameras at 34 km of altitude.

[48] More generally, the comparison of the bright spots from one methane window to the other (see Figure 5) implies a similar spectral behavior for all of them. All the bright regions stay bright, and all the dark areas stay dark. This spectral response of the bright spots is compatible with methane or hydrocarbon ice, which is always bright at all the considered wavelengths. This is a suggestion we have made previously based on data from 1998–2004 [*Coustenis et al.*, 2001, 2005]. As far as the photometry is concerned, though it is not strictly applicable to deconvolved images, we witness a decrease of the surface signal as the wavelength increases, something compatible with water ice, as reported also by DISR [*Tomasko et al.*, 2005].

5. Conclusions and Discussion

[49] At the time of the Huygens probe’s descent into Titan’s atmosphere, our team acquired adaptive optics images of Saturn’s satellite, so as to build the best diagnostic of its surface and atmosphere to be compared to the “ground truth” depicted by the probe.

[50] On two consecutive nights (15 and 16 January 2005), we observed Titan with the adaptive optics near infrared instrument NACO at the VLT. Three different imaging modes (Narrow-Band imaging, Simultaneous Differential Imager, Fabry-Pérot Imager) were successively used in excellent seeing conditions (0.6 arc sec), returning high-spatial resolution images of Titan’s atmosphere and surface between 1.28 and 2.2 μm . The contrast of all these images is also enhanced by deconvolution, and the atmosphere is characterized through the use of a radiative transfer model

[Rannou *et al.*, 2003]. The Huygens landing site is close to the center of our images, at best acquired with a 320-km spatial resolution at 1.28 μm . The FP mode, on the other hand, returns the best altitude sampling, extracting information from kilometer-thick layers of the atmosphere in the K band, between 2.00 and 2.20 μm .

[51] Many atmospheric phenomena were reported in the previous years by numerous teams: the north-south asymmetry pertaining to the different aerosol distribution from one hemisphere to the other (opposing the winter hemisphere to the summer one) was changing in the last 5 years [Lorenz *et al.*, 1999; Hirtzig *et al.*, 2006] and is now completely reversed [Ádámkóvics *et al.*, 2006]; at all available wavelengths, the northern limb is nowadays the brightest.

[52] In January 2005, shortly after Saturn's opposition, the solar phase angle was fairly weak (less than 0.6° , 10 times smaller than the usual phase values visible from Earth). The corresponding phase effect was expected on the evening (eastern) limb, yet on several images (the NB ones in particular) we detected an increase in luminosity on the morning (western) limb, due to a local increase of atmospheric aerosols that condensed in the stratosphere during Titan's night, as proposed by Coustenis *et al.* [2001] and Hirtzig *et al.* [2006]. The FP data should help us to discriminate the exact altitude of this phenomenon. Since the in-depth analysis has not been finished, we only can confirm that there is indeed such a trend in the stratosphere.

[53] After all these years, the nature of Titan's clouds is still a sensitive issue. Meanwhile, many transient clouds have been reported [Roe *et al.*, 2002a; Bouchez, 2004; Gibbard *et al.*, 2003; Porco *et al.*, 2005], and a large cloud system was confirmed above Titan's south pole [Griffith *et al.*, 1998; Porco *et al.*, 2005; Schaller *et al.*, 2005; Hirtzig *et al.*, 2006]; yet we have never observed the former and the latter which we have monitored almost from the beginning of its appearance is nowhere seen on our images taken in the year 2005. Within error bars, we barely detect a feeble feature at 2.11 μm , too weak to ascertain its presence. We can hence infer that this atmospheric phenomenon only lasted about one Titan season. On the contrary, one of the companions of this large system, detected usually on the limbs, is still obvious on the western limb: these companions were interpreted in one theory as the signature of a polar cap of stratosphere haze swept away from the Equator by the whole atmosphere dynamics [Hirtzig *et al.*, 2006], but there is no certain evaluation of their nature. The clouds over the south pole have disappeared, but not the layers of haze. This will be a further constraint on the atmosphere models.

[54] As far as the surface is concerned, we studied the contrast differentiating the various bright and dark patches visible on Titan's disc after the suppression of the atmospheric contribution signal. The comparison of the 1.28 (NB), 1.6 (SDI), and 2.0 (NB and FP) μm surface images shows that the contrast between bright and dark patches steadily increases as a function of wavelength. The Bright/Dark ratio indeed returns values of 2.0, 2.5 and 2.8 respectively. This will be helpful for determining the chemical components that change the spectral behavior of both these zones as done by Coustenis *et al.* [2005], with

mixtures of methane and water ices. We will expand this study in the future with broader ranges of surface materials, with mixtures of various ices and different sizes of grain, and compare the results to the ones obtained by other teams, like Zarnecki *et al.* [2005], Tomasko *et al.* [2005], and Rodriguez *et al.* [2006] from DISR or VIMS data.

[55] The Huygens landing site is located between a bright and a dark region. Our 320-km spatial resolution spans a large gradient of luminosity, so that we estimate the relative intensity of the area to be 0.7 ± 0.1 (given the brightest area will have a relative intensity of 1.0). The Huygens' region is fairly intermediate in brightness with respect to the darkest and brightest areas on our maps, but closer to the darker areas in this image of Titan's trailing side.

[56] Our results in this paper will hopefully allow to optimize the return from the instruments of the Cassini-Huygens mission. Having investigated in-depth only one location of Titan's disc, some extrapolation will be required to infer the surface composition at other locations. Ground-based images, maps and those gathered by the Cassini ISS, combined with RADAR measurements and other data may allow us to do so in the near future.

[57] **Acknowledgments.** The data presented here are based on observations collected at the European southern Observatory, Chile (ESO proposal 74.E-0747 for guarantee time with NACO). A. Negrão is supported by the FCT Ph.D. scholarship SFRH/BD/8006/2002. We thank M. E. Brown and an anonymous referee for their constructive advice.

References

- Ádámkóvics, M., I. de Pater, M. Hartung, F. Eisenhauer, R. Genzel, and C. A. Griffith (2006), Titan's bright spots: Multiband spectroscopic measurement of surface diversity and hazes, *J. Geophys. Res.*, *111*, E07S06, doi:10.1029/2005JE002610.
- Bouchez, A. H. (2004), Seasonal trends in Titan's atmosphere: Haze, wind, and clouds, Ph.D. thesis, Calif. Inst. of Technol., Pasadena.
- Bouchez, A. H., and M. E. Brown (2005), Statistics of Titan's south polar tropospheric clouds, *Astrophys. J.*, *618*, L53–L56.
- Bratsolis, E., and M. Sigelle (2001), A spatial regularization method preserving local photometry for Richardson-Lucy restoration, *Astron. Astrophys.*, *375*, 1120–1128.
- Brown, M. E., A. H. Bouchez, and C. A. Griffith (2002), Direct detection of variable tropospheric clouds near Titan's south pole, *Nature*, *420*, 795–797.
- Caldwell, J., et al. (1992), Titan: Evidence for seasonal change—A comparison of Hubble Space Telescope and Voyager images, *Icarus*, *97*, 1–9.
- Combes, M., L. Vapillon, E. Gendron, A. Coustenis, O. Lai, R. Witteberg, and R. Sirdey (1997), Spatially resolved images of Titan by means of adaptive optics, *Icarus*, *129*, 482–497.
- Coustenis, A., et al. (2001), Images of Titan at 1.3 and 1.6 μm with Adaptive Optics at the CFHT, *Icarus*, *154*, 501–515.
- Coustenis, A., et al. (2005), Maps of Titan's surface from 1 to 2.5 μm , *Icarus*, *177*, 89–105, doi:10.1016/j.icarus.2005.03.012.
- Coustenis, A., et al. (2006), Titan's 3-micron spectral region from ISO high-resolution spectroscopy, *Icarus*, *180*, 176–185, doi:10.1016/j.icarus.2005.08.007.
- Gendron, E., et al. (2004), VLT/NACO adaptive optics imaging of Titan, *Astron. Astrophys.*, *417*, L21–L24.
- Gibbard, S. G., B. Macintosh, D. Gavel, C. E. Max, I. de Pater, A. M. Ghez, E. F. Young, and C. P. McKay (1999), Titan: High-resolution speckle images from the Keck Telescope, *Icarus*, *139*, 189–201.
- Gibbard, S. G., I. de Pater, B. A. Macintosh, A. Grossman, and M. Adamkóvics (2003), Spatially-Resolved 2 micron Spectroscopy of Titan from the W. M. Keck Telescope, *Bull. Am. Astron. Soc.*, *35*, 931.
- Gibbard, S. G., B. Macintosh, D. Gavel, C. E. Max, I. de Pater, H. G. Roe, A. M. Ghez, E. F. Young, and C. P. McKay (2004), Speckle imaging of Titan at 2 microns: surface albedo, haze optical depth, and tropospheric clouds 1996–1998, *Icarus*, *169*, 429–439.
- Griffith, C. A., T. Owen, and R. Wagener (1991), Titan's surface and troposphere, investigated with ground-based, near-infrared observations, *Icarus*, *93*, 362–378.
- Griffith, C. A., T. Owen, G. A. Miller, and T. Geballe (1998), Transient clouds in Titan's lower atmosphere, *Nature*, *395*, 575–578.

- Griffith, C. A., T. Owen, T. R. Geballe, J. Rayner, and P. Rannou (2003), Evidence for the Exposure of Water Ice on Titan's Surface, *Science*, *300*, 628–630.
- Griffith, C. A., et al. (2005), The evolution of Titan's mid-latitude clouds, *Science*, *310*, 474–477, doi:10.1126/science.1117702.
- Hartung, M., T. M. Herbst, L. M. Close, R. Lenzen, W. Brandner, O. Marco, and C. Lidman (2004a), A new VLT surface map of Titan at 1.575 microns, *Astron. Astrophys.*, *421*, L17–L20.
- Hartung, M., C. Lidman, N. Ageorges, O. Marco, M. E. Kasper, and Y. Clenet (2004b), Commissioning of the NACO Fabry-Perot interferometer at the VLT, in *Ground-Based Instrumentation for Astronomy*, edited by A. F. Moorwood, and M. Iye, *Proc. SPIE*, *5492*, 1531–1541.
- Hartung, M., T. M. Herbst, C. Dumas, and A. Coustenis (2006), Limits to the abundance of surface CO₂ ice on Titan, *J. Geophys. Res.*, *111*, E07S09, doi:10.1029/2005JE002642.
- Hirtzig, M., A. Coustenis, E. Gendron, P. Drossart, A. Negrão, M. Combes, O. Lai, P. Rannou, S. Lebonnois, and D. Luz (2006), Monitoring atmospheric phenomena on Titan, *Astron. Astrophys.*, *456*(2), 761–774.
- Irwin, P. G. J., L. A. Sromovsky, E. K. Strong, K. Sihra, N. Bowles, S. B. Calcutt, and J. J. Remedios (2006), Improved near-infrared methane band models and k-distribution parameters from 2000 to 9500 cm⁻¹ and implications for interpretation of outer planet spectra, *Icarus*, *181*, 309–319.
- Lebreton, J. P., D. L. Matson, and The Huygens Team (2005), An overview of the descent and landing of the Huygens probe on Titan, *Nature*, *438*, 758–764.
- Lellouch, E., B. Schmitt, A. Coustenis, and J.-G. Cuby (2004), Titan's 5-micron lightcurve, *Icarus*, *168*, 209–214.
- Lenzen, R., et al. (2003), NAOS-CONICA first on sky results in a variety of observing modes, in *Instrument Design and Performance for Optical/Infrared Ground-based Telescopes*, edited by M. Iye and A. F. M. Moorwood, *Proc. SPIE*, *4841*, 944–952.
- Lenzen, R., L. Close, W. Brandner, B. Biller, and M. Hartung (2004), A novel simultaneous differential imager for the direct imaging of giant planets, in *Ground-Based Instrumentation for Astronomy*, edited by A. F. Moorwood and M. Iye, *Proc. SPIE*, *5492*, 970–977.
- Lorenz, R. D., M. T. Lemmon, P. H. Smith, and G. W. Lockwood (1999), Seasonal change on Titan observed with the Hubble Space Telescope WFPC-2, *Icarus*, *142*, 391–401.
- Magain, P., F. Courbin, and S. Sohy (1998), Deconvolution with correct sampling, *Astrophys. J.*, *494*, 472, doi:10.1086/305187.
- McKay, C. P., J. B. Pollack, and R. Courtin (1989), The thermal structure of Titan's atmosphere, *Icarus*, *80*, 23–53.
- Meier, R., B. A. Smith, T. C. Owen, and R. J. Terrile (2000), The surface of Titan from NICMOS observations with the Hubble Space Telescope, *Icarus*, *145*, 462–473.
- Negrão, A., A. Coustenis, E. Lellouch, J.-P. Maillard, P. Rannou, B. Schmitt, C. P. McKay, and V. Boudon (2006), Titan's surface albedo variations over a Titan season from near-infrared CFHT/FTS spectra, *Planet. Space Sci.*, *54*, 1225–1246.
- Negrão, A., M. Hirtzig, A. Coustenis, E. Gendron, P. Drossart, P. Rannou, M. Combes, and V. Boudon (2007), The 2- μ m spectroscopy of Huygens probe landing site on Titan with VLT/NACO, *J. Geophys. Res.*, doi:10.1029/2005JE002651, in press.
- Perryman, M. A. C., et al. (1997), The HIPPARCOS catalogue, *Astron. Astrophys.*, *323*, L49–L52.
- Pollack, J. B., and C. P. McKay (1985), The impact of polar stratospheric clouds on the heating rates of the winter polar stratosphere, *J. Atmos. Sci.*, *42*, 245–262.
- Porco, C. C., et al. (2005), Imaging of Titan from the Cassini spacecraft, *Nature*, *434*, 159–168.
- Rannou, P., C. P. McKay, and R. D. Lorenz (2003), A model of Titan's haze of fractal aerosols constrained by multiple observations, *Planet. Space Sci.*, *51*, 963–976.
- Rodriguez, S., S. Le Mouélic, C. Sotin, H. Clénet, R. N. Clark, B. Buratti, R. H. Brown, T. B. McCord, and VIMS Team (2006), CASSINI/VIMS hyperspectral observations of the Huygens landing site on Titan, *Planet. Space Sci.*, doi:10.1016/j.pss.2006.06.016, in press.
- Roe, H. G., I. de Pater, B. A. Macintosh, S. G. Gibbard, C. E. Max, and C. P. McKay (2002a), NOTE: Titan's atmosphere in late southern spring observed with adaptive optics on the W. M. Keck II 10-meter telescope, *Icarus*, *157*, 254–258.
- Roe, H. G., I. de Pater, B. A. Macintosh, and C. P. McKay (2002b), Titan's clouds from Gemini and Keck Adaptive Optics Imaging, *Astrophys. J.*, *581*, 1399–1406.
- Roe, H. G., I. de Pater, S. G. Gibbard, B. A. Macintosh, C. E. Max, E. F. Young, M. E. Brown, and A. H. Bouchez (2004), A new 1.6-micron map of Titan's surface, *Geophys. Res. Lett.*, *31*, L17S03, doi:10.1029/2004GL019871.
- Roe, H. G., A. H. Bouchez, C. A. Trujillo, E. L. Schaller, and M. E. Brown (2005), Discovery of temperate latitude clouds on Titan, *Astrophys. J.*, *618*, L49–L52.
- Rousset, G., et al. (2003), NAOS, the first AO system of the VLT: on-sky performance, in *Adaptive Optical System Technologies II*, edited by P. L. Wizinowich and D. Bonaccini, *Proc. SPIE*, *4839*, 140–149.
- Saint-Pé, O., M. Combes, F. Rigaut, M. Tomasko, and M. Fulchignoni (1993), Demonstration of adaptive optics for resolved imagery of solar system objects—Preliminary results on Pallas and Titan, *Icarus*, *105*, 263.
- Schaller, E. L., M. E. Brown, A. H. Bouchez, H. G. Roe, and C. A. Trujillo (2004), Continuous monitoring of Titan for large cloud outbursts, *Bull. Am. Astron. Soc.*, *36*, 1076.
- Schaller, E. L., M. E. Brown, H. G. Roe, A. H. Bouchez, and C. A. Trujillo (2005), Cloud activity on Titan during the Cassini Mission, paper presented at 36th Annual Lunar and Planetary Science Conference, Lunar and Planet. Inst., League City, Tex., 14–18 March.
- Smith, P. H., M. T. Lemmon, R. D. Lorenz, L. A. Sromovsky, J. J. Caldwell, and M. D. Allison (1996), Titan's surface, revealed by HST imaging, *Icarus*, *119*, 336–349.
- Tomasko, M. G., B. Archinal, T. Becker, and B. Bézard, et al. (2005), Rain, winds and haze during the Huygens probe's descent to Titan's surface, *Nature*, *438*, 765–778.
- Zarnecki, J. C., et al. (2005), A soft solid surface on Titan as revealed by the Huygens Surface Science Package, *Nature*, *438*, 792–795.

A. Coustenis, M. Combes, P. Drossart, and E. Gendron, LESIA, Observatoire de Paris-Meudon, F-92195 Meudon Cedex, France.
 M. Hartung, European Southern Observatory, Alonso de Cordova 3107 Casilla 19001 Santiago 19, Chile.
 M. Hirtzig, Laboratoire de Planétologie et de Géodynamique Faculté des Sciences, 2 rue de la Houssinière BP 92 208, F-44322 Nantes Cedex 03, France. (mathieu.hirtzig@univ-nantes.fr)
 A. Negrão and P. Rannou, Service d'Aéronomie du CNRS, Université de Versailles St-Quentin, BP3, F-91371 Verrières le Buisson, France. (pra@aerov.jussieu.fr)